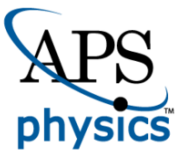

Local self-energies for V and Pd emergent from a nonlocal LDA+FLEX implementation

Sergey Y. Savrasov, Giacomo Resta, and Xiangang Wan

Phys. Rev. B **97**, 155128 — Published 13 April 2018

DOI: 10.1103/PhysRevB.97.155128

Local Self–Energies for V and Pd Emergent from a Non–Local LDA+FLEX Implementation

Sergey Y. Savrasov, Giacomo Resta
Department of Physics, University of California, Davis, CA 95616, USA

Xiangang Wan
National Laboratory of Solid State Microstructures and Department of Physics, Nanjing University, Nanjing 210093, China and Collaborative Innovation Center of Advanced Microstructures, Nanjing University, Nanjing 210093, China

In the spirit of recently developed LDA+U and LDA+DMFT methods we implement a combination of density functional theory in its local density approximation (LDA) with a k– and $\omega-$dependent self–energy found from diagrammatic fluctuational exchange (FLEX) approximation. The active Hilbert space here is described by the correlated subset of electrons which allows to tremendously reduce the sizes of matrices needed to represent charge and spin susceptibilities. The method is perturbative in nature but accounts for both bubble and ladder diagrams and accumulates the physics of momentum resolved spin fluctuations missing in such popular approach as GW. As an application, we study correlation effects on band structures in V and Pd. The d–electron self–energies emergent from this calculation are found to be remarkably k–independent. However, when we compare our calculated electronic mass enhancements against LDA+DMFT, we find that for the long standing problem of spin fluctuations in Pd, LDA+FLEX delivers a better agreement with experiment, although this conclusion depends on a particular value of Hubbard U used in the simulation. We also discuss outcomes of a recently proposed combinations of k–dependent FLEX with DMFT.

PACS numbers:

I. I. INTRODUCTION

Although electronic structure calculations utilizing a combination of local density functional and dynamical mean field theories (so called LDA+DMFT) became a method of choice for studying realistic correlated electrons systems[1], the search for a more accurate treatment of the electron self–energy continues to be an active field in the many–particle physics of condensed matter. Since DMFT accounts for local electronic correlations by corresponding solution of the Anderson impurity problem, extensions of this method to small clusters, such as Dynamical Cluster Approximation (DCA)[2] or cellular version of DMFT (C–DMFT)[3] have been proposed in the past and more recently, two promising developments, a dual fermion (DF) approach[4] and a dynamical vertex approximation (DΓA)[5], have been elaborated. Unfortunately, combinations of these approaches with LDA and their applications to real materials are complex, time consuming and have so far been scarce[6].

One recent development is the combination[7] of the DMFT with the much celebrated GW approach[8] that, in contrast to LDA+DMFT, tries to treat dynamically screened Coulomb interaction from first principles using a summation of a series of the particle–hole bubble diagrams, and does not rely on any *ad hoc* parametrizations such as "Hubbard U". Another advantage of the method is the treatment of the local self–energy using DMFT and the access to its k–dependence via the use of the GW diagram. Interestingly however, that GW itself misses an important physics associated with a well–known electronic mass renormalization due to paramagnons which has been recovered in the summation of the so called particle–hole ladder diagrams long time ago[9]. Thus, including both the bubble and ladder diagrams in a unified way with DMFT may provide more accurate interpolation for the k–dependence of the self–energy.

There was indeed a very long interest in such development. The paramagnons or spin fluctuations (SF) were originally shown to suppress electron–phonon pairing in conventional superconductors[10] but capable of producing d–wave pairing in unconventional superconductors[11,12]. The proposed Fluctuational Exchange Approximation (FLEX)[13] includes both particle–hole ladders and bubbles as well as particle–particle ladder diagrams, with the latter contribution being found of lesser importance at least in some models[14]. It was the method of choice in many studies of strongly correlated systems in the past[15]. A proposal to combine FLEX with LDA in a form of a LDA++ method came out in the earlier days of the LDA+DMFT developments[16]. Very recently, a combination of FLEX and DMFT on the level of a single–band Hubbard model in 2D was shown to reproduce a dome–like behavior of critical temperatures characteristic of cuprates superconductors[17].

Unfortunately, a completely first principles treatment of the ladder diagrams represents a challenge. First, the response functions in such theory are all four–point functions in real space and not two–point functions as in the GW method. Second, and most important, it has long been recognized that it is not the bare Coulomb but some semi–phenomenological Stoner–like interaction I should represent the short–range repulsion between correlated electrons in the ladder series[9]. The access to this quan-

tity within local density functional theory has allowed to compute spin fluctuational spectra together with paramagnon enhanced self–energies in V and Pd[18]. A more recent formulation of the method using all–electron basis sets and accurate summations over unoccupied states[19] has also allowed a few applications to selected transition metals[20].

Despite earlier excitement, the LDA based approaches to spin fluctuations did not receive a wider recognition because being a homogeneous electron gas theory LDA may seriously underestimate I for many correlated systems, and it has been stressed that the Hubbard parameter U should be used instead[21]. This gave rise to a famous LDA+U method[22].

In the absence of a first principles treatment of the interaction that enters the ladder diagrams we still have to rely on parametrizations in terms of U. However, the remaining part of the algorithm is implementable in principle: the FLEX self–energies for correlated electrons, $\Sigma^{FLEX}(\mathbf{k},\omega)$ can be computed using contributions from both bubble and ladder diagrams, and subsequently combined with LDA using a method of projectors. This is exactly as it is done in LDA+U and LDA+DMFT. Furthermore, the method can be extended by adding DMFT, as it has been recently shown for models[17,23]. The k–dependent corrections within such method are attributed to the diagrammatic FLEX which captures the important physics of spin fluctuations and is simpler to implement than recently proposed DF and DΓA approaches. As the danger of partial diagrammatic summations was pointed out in a recent work[23] we bear in mind that such schemes are perturbative in spirit and should not be literally used for any U.

In this work we describe an implementation of such method and provide applications to V and Pd. It is quite remarkable that the non–local FLEX self–energies that we extract in our implementation are fairly k–independent which justifies the use of local approximations. We calculate the mass enhancements of the d–electrons and compare them against LDA+DMFT calculations performed using numerically exact Continuous Time Quantum Monte Carlo (QMC) method[24] and other published DMFT calculations[25]. We find that FLEX delivers larger electronic masses than DMFT and agrees better with experiment, however, this conclusion depends on the value of U that is used in the simulation. We also comment on the performance of recently proposed DMFT+FLEX schemes[17,23] to the problem of mass enhancement in these two metals.

The paper is organized as follows. In Section II, we provide a general description how the self–energy for correlated electrons is combined with LDA (SELDA family of methods) and give specific details about our FLEX implementation. Various forms of self–consistency conditions are also discussed. In Section III, our applications for V and Pd are described. In Section IV, we conclude with the perspective on possible applications of such method to other systems.

II. II. FAMILY OF SELDA METHODS

The family of approaches that combine the self–energy for correlated electrons with LDA (the SELDA family), relies on a separation of sites given by the positions $\{\tau\}$ inside the unit cell of the lattice onto uncorrelated and correlated sites denoted hereafter by the positions $\{\mathbf{t}\}$. The site dependent projector operators are introduced with the help of radial solutions $\phi_{at}(\mathbf{r}_t) = \phi_{lt}(r_t)i^l Y_{lm}(\hat{r}_t)$ (where $\mathbf{r}_t = \mathbf{r} - \mathbf{t}$) of the one–electron Schroedinger equation taken with a spherically symmetric part of the full potential.[26]. The Hibert space $\{a\}$ inside the designated correlated site $\mathbf{t}$ may further restrict the full orbital set by a subset of correlated orbitals, such, e.g., as 5 for $l = 2$ or 7 for $l = 3$. Here, we keep the spin index explicitly, therefore treat the non–local self–energy $\hat{\Sigma}_{\sigma\sigma'} \equiv \Sigma_{\sigma\sigma'}(\mathbf{r},\mathbf{r}',\omega)$ as the matrix in spin space. It is viewed in travelling wave representation

$$\Sigma^{\mathbf{k}}_{\sigma\sigma'}(\mathbf{r}_\tau,\mathbf{r}'_{\tau'},\omega) = \sum_R e^{i\mathbf{k}\mathbf{R}}\Sigma_{\sigma\sigma'}(\mathbf{r},\mathbf{r}'-\mathbf{R},\omega) \quad (1)$$

as follows

$$\Sigma^{\mathbf{k}}_{\sigma\sigma'}(\mathbf{r}_\tau,\mathbf{r}'_{\tau'},\omega) = \delta_{\tau t}\delta_{\tau' t'}\sum_{aa'}\phi_{at}(\mathbf{r}_t)\Sigma^{corr}_{a\sigma t a'\sigma' t'}(\mathbf{k},\omega)\phi^*_{a' t'}(\mathbf{r}'_{t'}), \quad (2)$$

and is only non–zero when the legs $\mathbf{r}$ $\mathbf{r}'$ land inside the correlated sites. A single–particle LDA Hamiltonian with relativistic Pauli term is a 2x2 matrix operator

$$\hat{H}_{\sigma\sigma'} = -\nabla^2\delta_{\sigma\sigma'} + V^{LDA}_{\sigma\sigma'}(\mathbf{r}). \quad (3)$$

Since LDA potential already includes correlations in some average form, there exists a site diagonal double counting term $V^{DC(t)}_{a\sigma a'\sigma'}$ which has to be subtracted from the self–energy $\Sigma^{corr}_{a\sigma t a'\sigma' t'}(\mathbf{k},\omega)$ in Eq.(2). There is a vast literature about it, therefore here we ignore this subject and refer the reader to a recent work and references therein[27].

We represent the Green function of the lattice in terms of some, possibly non–orthonormal, basis set $\chi^{\mathbf{k}}_{\alpha\tau}(\mathbf{r})$, such as the one used in a full potential multiple–κ linear muffin–tin orbital (LMTO) method[28], as follows

$$G^{\mathbf{k}}_{\sigma\sigma'}(\mathbf{r},\mathbf{r}',\omega) = \sum_{\alpha\tau\alpha'\tau'}\chi^{\mathbf{k}}_{\alpha\tau}(\mathbf{r})G_{\alpha\sigma\tau\alpha'\sigma'\tau'}(\mathbf{k},\omega)\chi^{\mathbf{k}*}_{\alpha'\tau'}(\mathbf{r}'). \quad (4)$$

The inverse of the interacting Green function is the matrix

$$\begin{aligned} G^{-1}_{\alpha\sigma\tau\alpha'\sigma'\tau'}(\mathbf{k},\omega) &= \langle\chi^{\mathbf{k}}_{\alpha\tau}|(\omega+\epsilon_F)\delta_{\sigma\sigma'} - \hat{H}_{\sigma\sigma'} - \hat{\Sigma}_{\sigma\sigma'} + \hat{V}^{DC}_{\sigma\sigma'}|\chi^{\mathbf{k}}_{\alpha'\tau'}\rangle \\ &= (\omega+\epsilon_F)O^{\mathbf{k}}_{\alpha\sigma\tau\alpha'\sigma'\tau'} - H^{\mathbf{k}}_{\alpha\sigma\tau\alpha'\sigma'\tau'} - \Sigma^{\mathbf{k}}_{\alpha\sigma\tau\alpha'\sigma'\tau'}(\omega) + V^{\mathbf{k},DC}_{\alpha\sigma\tau\alpha'\sigma'\tau'}. \end{aligned} \quad (5)$$

It is expressed via the matrix elements of the LDA Hamiltonian, the overlap matrix, the correlated block of the self–energy $\Sigma^{corr}_{a\sigma ta'\sigma't'}(\mathbf{k},\omega)$ and of the double counting potential, as follows

$$H^{\mathbf{k}}_{\alpha\sigma\tau\alpha'\sigma'\tau'} = \langle\chi^{\mathbf{k}}_{\alpha\tau}|\hat{H}_{\sigma\sigma'}|\chi^{\mathbf{k}}_{\alpha'\tau'}\rangle, \quad (6)$$

$$O^{\mathbf{k}}_{\alpha\sigma\tau\alpha'\sigma'\tau'} = \delta_{\sigma\sigma'}\langle\chi^{\mathbf{k}}_{\alpha\tau}|\chi^{\mathbf{k}}_{\alpha'\tau'}\rangle, \quad (7)$$

$$\Sigma^{\mathbf{k}}_{\alpha\sigma\tau\alpha'\sigma'\tau'}(\omega) = \sum_{ata't'}\langle\chi^{\mathbf{k}}_{\alpha\tau}|\phi_{at}\rangle\Sigma^{corr}_{a\sigma ta'\sigma't'}(\mathbf{k},\omega)\langle\phi_{a't'}|\chi^{\mathbf{k}}_{\alpha'\tau'}\rangle, \quad (8)$$

$$V^{\mathbf{k},DC}_{\alpha\sigma\tau\alpha'\sigma'\tau'} = \sum_{aa'}\langle\chi^{\mathbf{k}}_{\alpha\tau}|\phi_{at}\rangle V^{DC(t)}_{a\sigma a'\sigma'}\langle\phi_{a't}|\chi^{\mathbf{k}}_{\alpha'\tau'}\rangle. \quad (9)$$

We note that the k–dependence of the matrix element $\Sigma^{\mathbf{k}}_{\alpha\sigma\tau\alpha'\sigma'\tau'}(\omega)$ comes here from both the non–trivial behavior for $\Sigma^{corr}_{a\sigma ta'\sigma't'}(\mathbf{k},\omega)$ as well as from the projector $\langle\chi^{\mathbf{k}}_{\alpha}|\phi_{at}\rangle$. Therefore, even for methodologies utilizing the local approximations, such as LDA+U and LDA+DMFT, the corresponding poles of the single–particle Green functions acquire the k–dependence induced by the hybridization effects with non–interacting electrons.

Given the prescription for computing the matrix $\Sigma^{corr}_{a\sigma ta'\sigma't'}(\mathbf{k},\omega)$, the poles of the single–particle Green function can, for example, be analyzed by diagonalizing the non–hermitian matrix $H^{\mathbf{k}}_{\alpha\sigma\tau\alpha'\sigma'\tau'} + \Sigma^{\mathbf{k}}_{\alpha\sigma\tau\alpha'\sigma'\tau'}(\omega) - V^{\mathbf{k},DC}_{\alpha\sigma\tau\alpha'\sigma'\tau'}$ for each frequency ω with the help of its right and left eigenvectors

$$\sum_{\alpha'\sigma'\tau'}[H^{\mathbf{k}}_{\alpha\sigma\tau\alpha'\sigma'\tau'} + \Sigma^{\mathbf{k}}_{\alpha\sigma\tau\alpha'\sigma'\tau'}(\omega) - V^{\mathbf{k},DC}_{\alpha\sigma\tau\alpha'\sigma'\tau'} - p_{\mathbf{k}j}(\omega)O^{\mathbf{k}}_{\alpha\sigma\tau\alpha'\sigma'\tau'}]R^{\mathbf{k}j}_{\alpha'\sigma'\tau'}(\omega) = 0, \quad (10)$$

$$\sum_{\alpha\sigma\tau}L^{\mathbf{k}j}_{\alpha\sigma\tau}(\omega)[H^{\mathbf{k}}_{\alpha\sigma\tau\alpha'\sigma'\tau'} + \Sigma^{\mathbf{k}}_{\alpha\sigma\tau\alpha'\sigma'\tau'}(\omega) - V^{\mathbf{k},DC}_{\alpha\sigma\tau\alpha'\sigma'\tau'} - p_{\mathbf{k}j}(\omega)O^{\mathbf{k}}_{\alpha\sigma\tau\alpha'\sigma'\tau'}] = 0. \quad (11)$$

A. FLEX Self–Energy

The prescription for computing the matrix $\Sigma^{corr}_{a\sigma ta'\sigma't'}(\mathbf{k},\omega)$ within the subset of correlated electrons can be obtained by a variety of methods. The dynamical mean field theory uses a k–independent approximation: $\Sigma^{corr}_{a\sigma ta'\sigma't'}(\mathbf{k},\omega) \equiv \delta_{tt'}\Sigma^{DMFT(t)}_{a\sigma a'\sigma'}(\omega)$ and solves the corresponding Anderson impurity problem subjected to a self–consistency condition. The treatment of the substitutional site disorder can utilize a coherent potential approximation (CPA)[30], $\Sigma^{corr}_{a\sigma ta'\sigma't'}(\mathbf{k},\omega) \equiv \delta_{tt'}\Sigma^{CPA(t)}_{a\sigma a'\sigma'}(\mathbf{k},\omega)$, where the subset $\{a\}$ should, in principle, refer to all orbitals (not only the ones restricted by a particular angular momentum l) within the substituted site t of the lattice. The technique is similar to DMFT as it has been recently implemented for studies of surface vacancies in TaAs Weyl semimetal[31]. The fluctuational exchange approximation relies on the diagrammatic summation of the bubble and ladder diagrams: $\Sigma^{corr}_{a\sigma ta'\sigma't'}(\mathbf{k},\omega) \equiv \Sigma^{FLEX}_{a\sigma ta'\sigma't'}(\mathbf{k},\omega)$.

We now briefly describe our implementation for computing the FLEX self–energy. All calculations are performed on the real frequency axis at zero temperature ($T = 0$). We neglect the particle–particle ladders which are known to be small, at least for the problem of paramagnons where the most divergent term is given by the particle–hole ladders. Contrary to the bubble diagrams which are expressed via two–point functions in the real space, the ladder diagrams rely on the 4–point functions in general, but the use of the on–site Hubbard–type interactions allows one to express all quantities via the charge and spin (longitudinal and transverse) susceptibilities which are two–point functions. Despite this simplification gives the scaling with the number of atoms in the unit cell as $N^2_{\{\tau\}}$, it is still a computationally very demanding problem because the number of matrix elements for representing the susceptibility grows as $N^2_{\{\tau\}}N^4_{orb}$ where N_{orb} is the size of the complete orbital manifold per atom needed. This, for example, slows down the calculation of the GW method. However, the restriction by the correlated subset simplifies the calculation tremendously, because now the susceptibility matrices have the size $N^2_{\{t\}}N^4_{corr}$.

We now define the susceptibility within the correlated subset. It is represented by the convolution of two Green functions on the frequency axis

$$\pi_{a\sigma bst,b's'a'\sigma't'}(\mathbf{q},\omega) = -i\sum_{\mathbf{k}}\int_{-\infty}^{+\infty}\frac{d\omega'}{2\pi}G_{bstb's't'}(\mathbf{k}+\mathbf{q},\omega')G_{a'\sigma't'a\sigma t}(\mathbf{k},\omega+\omega')e^{i\omega'0^+}. \quad (12)$$

For the non–interacting (LDA) Green's functions

$$G_{a'\sigma't'a\sigma t}(\mathbf{k},\omega) \rightarrow G^{(0)}_{a'\sigma't'a\sigma t}(\mathbf{k},\omega) = \sum_j \frac{\langle \phi_{a't'}|\psi_{\mathbf{k}j\sigma'}\rangle\langle\psi_{\mathbf{k}ja}|\phi_{\sigma t}\rangle}{\omega - \epsilon_{\mathbf{k}j} - i0^+\mathrm{sign}(\epsilon_F - \epsilon_{\mathbf{k}j})}, \tag{13}$$

represented in the basis of the Bloch wave functions that diagonalize the LDA Hamiltonian

$$\psi_{\mathbf{k}j\sigma}(\mathbf{r}) = \sum_{\alpha\tau} A^{\mathbf{k}j}_{\alpha\sigma\tau}\chi^{\mathbf{k}}_{\alpha\tau}(\mathbf{r}), \tag{14}$$

$$0 = \sum_{\alpha'\sigma'\tau'} (H^{\mathbf{k}}_{\alpha\sigma\tau\alpha'\sigma'\tau'} - \epsilon_{\mathbf{k}j}O^{\mathbf{k}}_{\alpha\tau\alpha'\tau'})A^{\mathbf{k}j}_{\alpha'\sigma'\tau'}, \tag{15}$$

the resulting expression for susceptibility matrix elements is given by

$$\pi_{a\sigma bst,b's'a'\sigma't'}(\mathbf{q},\omega) = \sum_{\mathbf{k}jj'} \frac{\theta(\epsilon_F - \epsilon_{\mathbf{k}j}) - \theta(\epsilon_F - \epsilon_{\mathbf{k}+\mathbf{q}j'})}{\omega + \epsilon_{\mathbf{k}j} - \epsilon_{\mathbf{k}+\mathbf{q}j'} + i0^+\mathrm{sign}(\epsilon_F - \epsilon_{\mathbf{k}j}) - i0^+\mathrm{sign}(\epsilon_F - \epsilon_{\mathbf{k}+\mathbf{q}j'})} \times \langle\psi_{\mathbf{k}j\sigma}|\phi_{at}\rangle\langle\phi_{bt}|\psi_{\mathbf{k}+\mathbf{q}j's}\rangle\langle\psi_{\mathbf{k}+\mathbf{q}j's'}|\phi_{b't'}\rangle\langle\phi_{a't'}|\psi_{\mathbf{k}j\sigma'}\rangle. \tag{16}$$

We note that exactly as in the spirit of the LDA+U and LDA+DMFT methods, the index $a\sigma bs$ here describes the active Hilbert space of the atom t, where a and b are orbital while σ and s are spin degrees of freedom. For d–electrons its size is only $(5*2)^2 = 100$. This is much smaller of the full Hilbert space needed to describe the susceptibility matrix.

We next introduce the on–site Hubbard matrix $U^{(t)}_{aba'b'}$ which describes the Coulomb interaction matrix elements among correlated orbitals within a given atomic volume Ω_t

$$\langle\phi_a\phi_{a'}|\frac{e^2}{r}|\phi_b\phi_{b'}\rangle_{\Omega_t} = U^{(t)}_{aba'b'}. \tag{17}$$

We use such parametrization so that the screening effects in U can be taken into account by an external calculation or phenomenologically. It is useful to define the interaction as the difference between bare and exchange terms and introduce spin indexes explicitly so that the indexation matches the one for susceptibility

$$I_{a\sigma bst,a'\sigma'b's't'} = \delta_{tt'}[\delta_{\sigma s}\delta_{\sigma's'}U^{(t)}_{aba'b'} - \delta_{\sigma s'}\delta_{\sigma's}U^{(t)}_{ab'a'b}] \tag{18}$$

This allows to drop the indexation and manipulate with matrix products symbolically. Define the dielectric function matrix for the correlated subspace

$$\hat{\epsilon}(\mathbf{q},\omega) = \hat{1} - \hat{I}\hat{\pi}(\mathbf{q},\omega). \tag{19}$$

Its inverse gives rise to the interacting susceptibility

$$\hat{\chi}(\mathbf{q},\omega) = \hat{\pi}(\mathbf{q},\omega)\hat{\epsilon}^{-1}(\mathbf{q},\omega), \tag{20}$$

and to the dynamically screened interaction for the correlated manifold

$$\hat{K}(\mathbf{q},\omega) = \hat{I} + \hat{I}[\hat{\chi}(\mathbf{q},\omega) - \frac{1}{2}\hat{\pi}(\mathbf{q},\omega)]\hat{I}. \tag{21}$$

The subtraction of $\frac{1}{2}\hat{\pi}(\mathbf{q},\omega)$ takes care of the single bubble diagram that appears twice in both bubble and ladder series.

The FLEX self–energy appears as the integral over frequencies

$$\Sigma^{FLEX}_{a\sigma ta'\sigma't'}(\mathbf{k},\omega) = -\sum_{bb'}\sum_{ss'}\sum_{\mathbf{q}}\int_{-\infty}^{+\infty}\frac{d\omega'}{2\pi i}K_{a\sigma bst,b's'a'\sigma't'}(\mathbf{k}-\mathbf{q},\omega')G^{(0)}_{bstb's't'}(\mathbf{q},\omega+\omega')e^{i\omega'0^+}. \tag{22}$$

Here we have used the non–interacting LDA Green function $G^{(0)}$ within the correlated subset, Eq. (13). To evaluate the frequency integral in practice, we use spectral representation for the dynamically screened interaction K which allows to perform integration over frequencies analytically. This is similar how it is done in some GW implementations[8].

Finally, we check the Hartree–Fock limit and show that the FLEX self–energy goes exactly to the one used in the LDA+U method. Replace the interaction matrix by site diagonal, frequency and $\mathbf{q}$ independent matrix I in Eq.(22)

$$K_{a\sigma bst,a'\sigma'b's't'}(\mathbf{q},\omega) \to I_{a\sigma bst,a'\sigma'b's't'} \equiv \delta_{tt'} I^{(t)}_{a\sigma bs,a'\sigma'b's'}. \tag{23}$$

The frequency integral in Eq. (22) is performed by closing the contour in the upper plane due to $e^{i\omega' 0^+}$. Then, the only poles in the upper plane, (*i.e.* those corresponding to the occupied states), contribute and we obtain the definition of the density matrix for correlated electrons

$$\begin{aligned}\sum_{\mathbf{k}} \int_{-\infty}^{+\infty} \frac{d\omega'}{2\pi i} G^{(0)}_{bstb's't'}(\mathbf{k},\epsilon) e^{i\omega' 0^+} &= \sum_{\mathbf{k}j} \langle \phi_{bt}|\psi_{\mathbf{k}js}\rangle\langle\psi_{\mathbf{k}js'}|\phi_{b't'}\rangle \int_{-\infty}^{+\infty} \frac{d\omega'}{2\pi i} \frac{e^{i\omega' 0^+}}{\omega' - \epsilon_{\mathbf{k}j} - i0^+ \mathrm{sign}(\epsilon_F - \epsilon_{\mathbf{k}j})} \\ &= \sum_{\mathbf{k}j} \theta(\epsilon_F - \epsilon_{\mathbf{k}j}) \langle \phi_{bt}|\psi_{\mathbf{k}js}\rangle\langle\psi_{\mathbf{k}js'}|\phi_{b't'}\rangle = n_{b's't'bst}. \end{aligned} \tag{24}$$

The Hartree–Fock limit is now recovered

$$\begin{aligned}\Sigma^{FLEX}_{a\sigma ta'\sigma't'}(\mathbf{k},\omega) \;\to\; \Sigma^{LDA+U}_{a\sigma ta'\sigma't'} &= -\sum_{bb'}\sum_{ss'} I_{a\sigma bst,b's'a'\sigma't'} n_{b's't'bst} \\ &= \delta_{tt'} \sum_{bb'}\sum_{ss'} I^{(t)}_{a\sigma a'\sigma',b's'bs} n^{(t)}_{b's'bs}, \end{aligned} \tag{25}$$

where only site diagonal density matrix for the correlated electrons is needed

$$n^{(t)}_{b's'bs} = n_{b's'tbst}. \tag{26}$$

This Σ^{LDA+U} is used in the LDA+U method.

B. Note on Self–Consistency

We now comment on the self–consistency condition within this approach. First, due to the existence of generating functionals for both GW and FLEX approximations[8,13], it looks like the self–consistency with respect to the Green functions and the interactions has to be implemented. However, at least within the GW method the subject was studied in some details with applications to some real materials[32]. The short answer is that finding fully self–consistent solution within the bubble diagrams is not a good idea because while providing better total energies, it worsens the one–electron spectra. There is also a technical part of the problem that once the complex self–energy is introduced, the polarizability (12) can no longer be represented in its simple form (16) and alternative formulations via, for example, imaginary time axis need to be implemented.

The self–consistency is however an important step within DMFT as it allows to describe, for example, the Mott transition. One can easily combine the non–local FLEX self–energy with the DMFT local self–energy, in accord with the recent proposals[17,23]

$$\begin{aligned}\Sigma^{DMFT+FLEX}(\mathbf{k},\omega) &= \Sigma^{DMFT}(\omega) + \\ &\Sigma^{FLEX}(\mathbf{k},\omega) - \Sigma^{DC}(\omega) \end{aligned} \tag{27}$$

This allows to utilize sophisticated impurity solvers developed in DMFT community. Here, the subtracted double counting term $\Sigma^{DC}(\omega)$ utilizes the FLEX approximation itself as the impurity solver[17], where one calculates the local polarizability $\pi_{loc}(\omega) = \sum_q \pi(\mathbf{q},\omega)$ which is represented in this method as the product of the two local Green functions, that will subsequently appear in Eq. (12) once the summation over $\mathbf{q}$ is performed. Then, the local interaction, as in Eq. (21), is computed which gives rise to the local impurity self–energy within the FLEX approximation. We denote it hereafter as $\Sigma^{DC}(\omega) = \Sigma^{DMFT(FLEX)}(\omega)$. Another option for $\Sigma^{DC}(\omega)$ is to use the local FLEX self–energy[23]

$$\Sigma^{FLEX}_{loc}(\omega) = \sum_{\mathbf{k}} \Sigma^{FLEX}(\mathbf{k},\omega). \tag{28}$$

Note that DMFT(FLEX) approach has been recently applied to study the mass enhancement in Pd[25]. We discuss the outcomes of various approximations for the self–energy in V and Pd in the following section.

Another sort of self–consistency that was developed in the past is the quasiparticle self–consistency. That is when not the full self–energy but its value at $\omega = 0$ and its frequency derivative around $\omega = 0$ describing mass enhancement data are used to reconstruct new densities and resulting quasiparticle Green's functions. It was developed in connection with the GW approach, and was shown to reproduce the band gaps of semiconductors quite well[33]. A combination of the LDA and Gutzwiller's method (called LDA+G) explores a similar idea[34] where the variational Gutzwiller method is used to find those self–energy parameters. It was also implemented in a

most recent combination of the GW and DMFT called QSGW+DMFT[35].

It is fairly straightforward to implement this sort of self–consistency within the described LDA+FLEX method. The polarizability is still represented by its non–interacting form (16) since quasiparticle approximation for the Green functions assumes real eigenvalues. It is also easy to update the position of the Fermi level and restore the new density at each iteration which replaces the LDA density in Eq. (3). However, in our applications to V and Pd we did not find any noticeable changes in the obtained self–energies and the spectral functions for d–electrons when doing these updates, and the results obtained at first iteration by using the LDA band structures are already very close self–consistency. It would probably make more sense doing it when evaluating total energies but this topic is beyond the scope of the present work.

III. III. APPLICATIONS TO V AND PD

Here we describe applications of our LDA+FLEX implementation to V and Pd. These two elemental metals have been at the center of interest for a long time, and, in particular Palladium, whose strong spin fluctuations are known to destroy superconductivity[10] and contribute to specific heat renormalization by $\lambda \sim 0.3 - 0.4$[10,18,36,37]. Most recent LDA+DMFT study[25] addressed the mass enhancement of Pd in great detail but extracted smaller $\lambda = 0.03 - 0.09$ for the values of U ranging from 1 to 4 eV using LDA+DMFT method with the FLEX approximation as the impurity solver. Vanadium is known to be less paramagnetically enhanced and its specific heat renormalization may well be described electron–phonon interactions alone[37]. However, a room for spin–fluctuational contribution still exists as λ based on the FLEX calculated self–energy with Stoner–type LDA interaction strength was earlier found to be 0.2[18]. It is also known that one needs a pretty large value of the effective Coulomb pseudopotential $\mu^* \sim 0.3$ to adjust the superconducting critical temperature of V to the one known from experiment[37], part of which may be attributed to λ.

For our band structure calculational framework we use double–κ full potential LMTO method as implemented in Ref.[28]. Experimental lattice constants, touching muffin–tin spheres, and LDA parametrization of Ref.[29] are utilized. The Green functions, susceptibilities and interactions are computed on the grid of 400 frequencies and for 256 non–equivalent wave vectors set by (20,20,20) divisions of the reciprocal unit cell. All integrals over the BZ are performed using grids set by (60,60,60) divisions of the reciprocal unit cell with help of a version of the tetrahedron method adapted for linear response calculations[28].

As far as determining precise value of U for these materials, there is some obvious uncertainty here. One estimate can be given by associating it with the Stoner parameter which was calculated for these metals to be as small as 0.025 Ry (0.34 eV)[41]. The upper estimate can also be obtained from the Stoner criterion of magnetism, i.e. when the static interacting susceptibility as given by Eq. (20) diverges. We have analyzed eigenvalues of the wavevector dependent dielectric matrix, Eq. (19), at $\omega = 0$ in the active space of d–electrons and found that the negative eigenvalues appear at $U_c = 0.31$ Ry for V and at 0.26 Ry for Pd. These critical values should signalize that the system undergoes the spin density wave (SDW) transition within this approach. (The use of local quantities in Stoner criterion, *i.e.* the ones summed over $\mathbf{q}$, lead to $U_c = 0.43$ Ry for V and at 0.59 Ry for Pd). We perform all computations for a range of U values varying it from 0 to 0.2 Ry.

We now discuss our calculated d–electron self–energies. Our results for V and Pd are shown in Fig. 1 where we plot matrix elements of $\mathrm{Re}\Sigma^{FLEX}(\mathbf{k},\omega)$ and $\mathrm{Im}\Sigma^{FLEX}(\mathbf{k},\omega)$ for both T_{2g} and E_g electrons. Here we use some representative value of U=0.2 Ry (2.7 eV) but our conclusions remain the same for the whole range of U's that we studied. The Hartree Fock values for $\mathrm{Re}\Sigma$ are subtracted in both plots. To illustrate the k–dependence, the self–energies are given for several wave vectors k chosen along $(0\xi\xi)$ direction of the Brillouin Zone (BZ). It is remarkable that the k–dependence in these plots is quite small suggesting that the local self–energy approximation may be adequate. We also compared the self–energies for other k–points in the BZ and came up with a similar conclusion. We subsequently calculate the $\Sigma^{FLEX}_{loc}(\omega)$ as a sum over k–points whose frequency dependence is also visualized in Fig. 1 by small circles. We see a close agreement between $\Sigma^{FLEX}_{loc}(\omega)$ and $\Sigma^{FLEX}(\mathbf{k},\omega)$ for both T_{2g} and E_g matrix elements.

Based on our calculated d–electron self–energies $\Sigma^{FLEX}(\mathbf{k},\omega)$, we calculate poles of single particle Greens functions and plot the obtained $\mathrm{Im}G(\mathbf{k},\omega)$ for V and Pd in Fig. 2. Here we compare the results of our many–body calculation with the energy band structures obtained by LDA. Although many versions of the double counting potentials currently exist[27], to illustrate the $\mathbf{k}-$ and ω dependence of the FLEX self–energy we merely subtract from $\Sigma^{FLEX}(\mathbf{k},\omega)$ its local value, Eq. (28), at $\omega = 0$ in order to visualize $\mathrm{Im}G(\mathbf{k},\omega)$. As one sees, the primary effect of the self–energy is the renormalization of the d–electron bandwidth and a small broadening that is acquired by the d–electrons due to the appearance of the imaginary part of $\Sigma^{FLEX}(\mathbf{k},\omega)$. We use the same self–energies (calculated at U=0.2 Ry) as plotted in Fig. 1.

Note that although the present data suggests the notion of locality for the self–energy in real space, we draw this conclusion from the plots that are given at energy scale of ± 1 Ry (our Fig. 1), which is of course much larger of typical energies of paramagnons known to be strong in Pd. To verify the presence of spin fluctuations within our method, we have plotted the imaginary part of the interacting spin susceptibility for Pd at small fre-

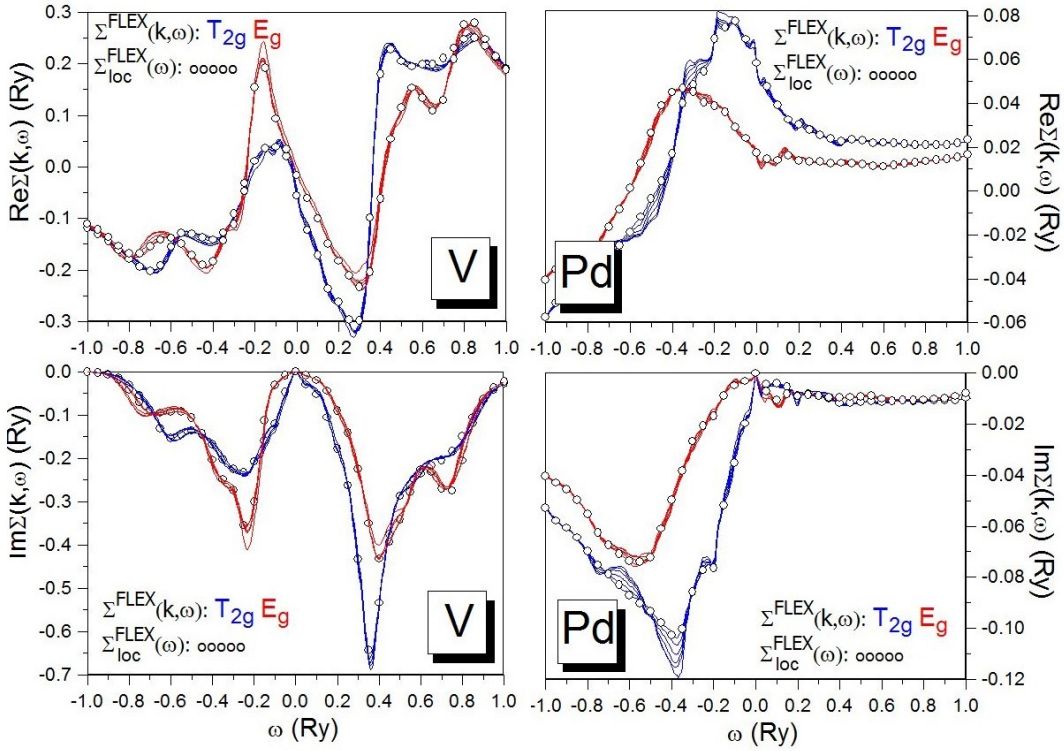

FIG. 1: Calculated self–energy $\Sigma(\mathbf{k},\omega)$ (top is the real part, and bottom is imaginary part) using FLEX approximation for t_{2g} and e_g electrons in V and Pd for the wavevector k traversing along $(0\xi\xi)$ direction of the Brillouin Zone. The circles show the result of the sum over all k–points representing the local FLEX self–energy. A representative value of Hubbard U=0.2 Ry is used in these plots, but the notion of locality persists for a whole range of U's.

quencies and for several wave vectors $\mathbf{q}$. The result is shown in Fig. 3 where one sees the divergent behavior of $\mathrm{Im}\chi(\mathbf{q},\omega)$ at frequencies $\lesssim 0.01$ Ry when $\mathbf{q}\to 0$ that is characteristic of damped ferromagnetic spin waves[18]. Zooming the precise behavior of the self–energy at this scale would be interesting in principle, but likely requires a lot more elaborated study with the full inclusion of temperature broadening in the simulation and understanding the role of the self–consistency within FLEX.

We now would like to compare the results of our calculations with the self–energies obtained using DMFT and directly with experiment. Unfortunately, the most accurate solvers developed to date are based on the Continuous Time Quantum Monte Carlo method (CT–QMC)[24], which work on imaginary time–frequency axis, and obtaining frequency dependence of the self–energy on the real axis involves an analytical continuation algorithm which is known to be not very accurate. However, one can easily perform calculations of correlation induced electronic mass enhancement in both metals using DMFT(QMC) since it can be extracted directly from the knowledge of $\Sigma^{DMFT(QMC)}(i\omega_n)$ on imaginary axis. The mass enhancement is then determined as the Fermi surface average of the frequency derivative of the self–energy taken at either $\omega=0$ or at $i\omega_n\to 0$. This is also a more sensitive way to compare various approximations for the self–energy.

In order to perform LDA+DMFT(QMC) calculations we downloaded Embedded DMFT code developed by Haule[38]: The LDA part of the code uses the full–potential Linear Augmented Plane Wave method (FP–LAPW) as implemented in the WIEN2k package[39]. A $\mathbf{k}$–grid of 26 x 26 x 26 divisions of the reciprocal unit cell and a plane–wave cutoff of $R_{MT}K_{max}=8$ were used in the LDA calculation. To deal with the DMFT impurity problem, cubic harmonics representation as a basis was utilized, and the CT–QMC solver based on hybridization expansion[40] was used at temperature $T=290K$ and 1909 Matsubara points on imaginary axis. The double–counting potential was determined under the "nominal" occupancy scheme[38] where a nominal valence of $n_d^{(0)}=3$ was used for the case of Vanadium and $n_d^{(0)}=10$ for Palladium.

Fig. 4 shows our calculated mass enhancements for V or Pd. To gain some physical insights on approximations used in these simulations, we choose to provide these data as a function of U. One can see that for small values of U both FLEX and DMFT give very similar mass enhancements. This is quite easy to understand because when U goes to zero, due to the emergent locality of the self–energy evident from Fig. 1, the FLEX provides a good approximation for solving the impurity

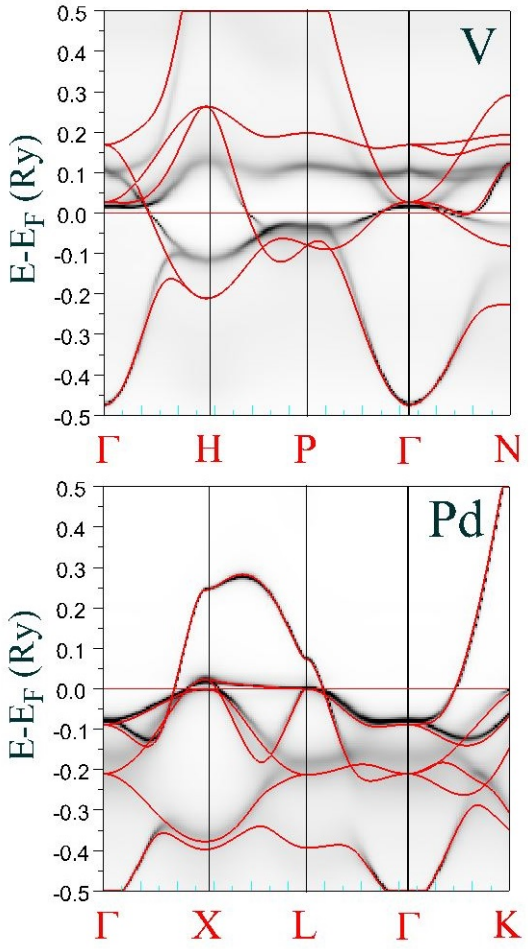

FIG. 2: Effect of FLEX self-energy on the calculated poles of single particle Green's functions for V and Pd as compared with their LDA band structures . The local FLEX value at $\omega = 0$ is subtracted from $\Sigma^{FLEX}(\mathbf{k},\omega)$ when visualizing Im$G(\mathbf{k},\omega)$. Hubbard U=0.2 Ry is used.

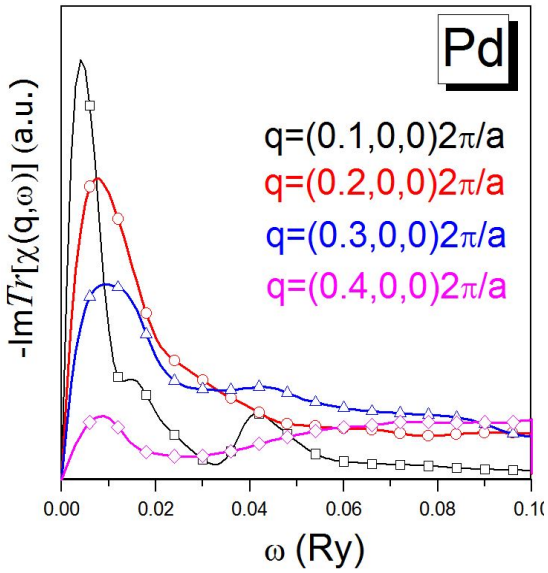

FIG. 3: Imaginary part of interacting susceptibility matrix (taken as sum of its diagonal matrix elements) for Pd plotted as a function of frequency for several wave vectors $\mathbf{q}$ =(ξ00)2π/a with ξ =0.1 (squares),0.2 (circles), 0.3(triangles), 0.4 (rhombs). Hubbard U=0.2 Ry is used.

problem while self–consistency imposed by DMFT is not essential[1]. However, as U increases, FLEX delivers significantly larger values of λ than DMFT. This can also be understood since we start approaching the spin density wave transition which occurs at $U_c = 0.31$ Ry for V and at 0.26 Ry for Pd within FLEX.

A recent publication addressed the specific heat renormalization in Pd using LDA+DMFT method with FLEX as the impurity solver. The deduced λ was found to be in the range $0.03 - 0.09$ for the values of U between 1 to 4 eV. This is in accord with our LDA+DMFT(QMC) simulation as seen from Fig. 4. At least within LDA+DMFT(FLEX), the result for such small mass enhancement can be understood from the Stoner argument, if we ignore DMFT self–consistency. The structure of the expression for the susceptibility is then RPA like, it is the same in both momentum–resolved and local cases. Then the use of the local susceptibilities instead of momentum resolved ones in Eqs. (19)–Eq. (21) results in SDW instability at higher values of critical U (U_c=0.43 Ry for V and U_c=0.59 Ry for Pd) while our fixed value of U = 0.2 Ry produces less enhanced local interacting susceptibility and a smaller mass enhancement. Overall, the trends that we monitor here are pretty much expected from a vast amount of simulations performed on models[1]. Thus, one can conclude that from the standpoint of the comparison with the experiment, both DMFT(QMC) and DMFT(FLEX) calculations underestimate the mass enhancement of Pd, while our full momentum resolved FLEX implementation is capable to provide a more reliable estimate, at least for the range of the values of U employed in the present study. One can speculate that FLEX still gives an unreliable result while DMFT needs a significantly larger value of U to deal with this problem but the possibility of magnetic ordering transition at larger U's should not be overlooked. Another option is the need for self–consistent treatment of spin fluctuations and electron–phonon interactions while extracting the specific heat renormalization but this study is well beyond the scope of the present work.

One can finally comment on the results of a recently proposed DMFT+FLEX scheme[17], Eq. (27). As a result of the weak coupling regime that we study here for V and Pd, we can approximate $\Sigma^{DMFT}(\omega)$ by $\Sigma^{DMFT(FLEX)}(\omega) = \Sigma^{DC}(\omega)$, and the mass enhancements that would be obtained within it will practically coincide with the ones that we find within FLEX itself. If, on the other hand, one uses[23] $\Sigma^{DC}(\omega) = \Sigma^{FLEX}_{loc}(\omega)$, Eq. (28), and because the d–electron self–energies $\Sigma^{FLEX}(\mathbf{k},\omega)$ are found to be well approximated

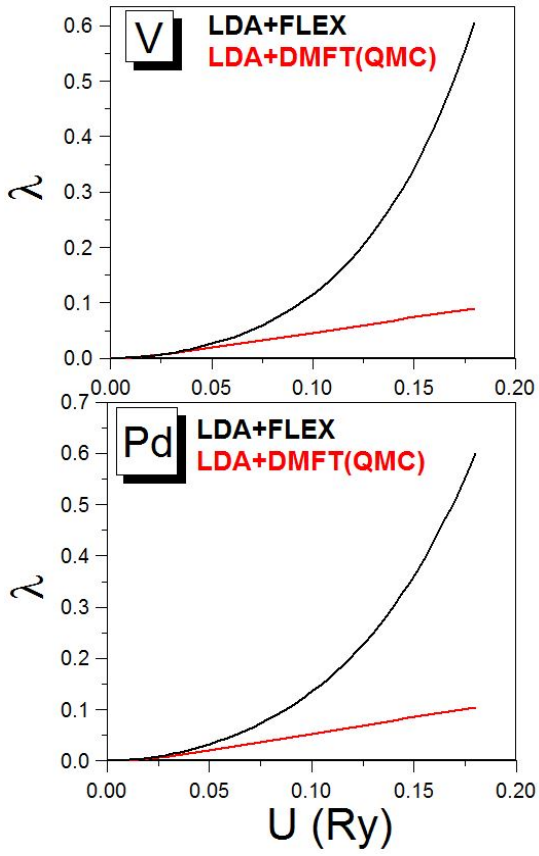

FIG. 4: Comparisons between LDA+FLEX and LDA+DMFT approximations for predicting correlation induced electronic mass enhancement factor λ in V and Pd. The calculations with Dynamical Mean Field Theory are performed using Quantum Monte Carlo method as implemented in Ref.[38].

by $\Sigma_{loc}^{FLEX}(\omega)$, the mass enhancements that would be obtained now will be the ones that we find from DMFT, thus bringing no advantage in such combination at least for the problem of Pd.

IV. IV. CONCLUSION

In conclusion, by implementing a combination of $\mathbf{k}-$ and $\omega-$ dependent self–energy found from fluctuational exchange approximation with LDA, we are able to incorporate the effect of momentum resolved spin fluctuations on the calculated single particle spectra of real materials. Applicability of the approach was demonstrated for two elemental metals, V and Pd whose self–energies have been found remarkably k–independent justifying the use of local approximations. However, we find corresponding mass enhancement data to be different when comparing the results of our calculations with local LDA+DMFT approach, where LDA+FLEX delivers better agreement with experiment for the range of values of $U \lesssim 0.2$ *Ry*. The method is naturally combinable with Dynamical Mean Field Theory which would allow to properly take into account all sorts of local excitations, including satellites, atomic multiplets, *etc.* that are frequently seen in photoemission spectra of real correlated systems. We are hoping that such extension may also provide additional clues on the electronic properties of unconventional superconductors, where one can track materials dependence of the superconductivity, which is somewhat lacking when addressing this problem using model Hamiltonians.

V. ACKNOWLEDGEMENT

The authors are indebted to Motoharu Kitatani for discussing the details of their DMFT+FLEX method. This work was supported by the US NSF DMR Grant No. 1411336. X. G. Wan was supported by NSF of China, Grant No. 11525417.

[1] For a review, see, e.g, G. Kotliar, S. Y. Savrasov, K. Haule, V. S. Oudovenko, O. Parcollet, C.A. Marianetti, Rev. Mod. Phys. **78**, 865-951, (2006).
[2] M. H. Hettler, M. Mukherjee, M. Jarrell, and H. R. Krishnamurthy, Phys. Rev. B **61**, 12739 (2000).
[3] G. Kotliar, S. Savrasov, G. Palsson, and G. Biroli, Phys. Rev. Lett. **87**, 186401 (2001).
[4] A. N. Rubtsov, M. I. Katsnelson, and A. I. Lichtenstein, Phys. Rev. B 77, 033101 (2008).
[5] A. Toschi, A. A. Katanin, and K. Held, Phys. Rev. B **75**, 045118 (2007).
[6] For recent applications, see, e.g., P. Sémon, K. Haule, and G. Kotliar, Phys. Rev. B 95, 195115 (2017).
[7] For a review, see, e.g, S. Biermann, J. Phys.: Condens. Matter. **26**, 173202 (2014)
[8] For a review, see, e.g, F. Aryasetiawan, O. Gunnarsson, Rep. Prog. Phys. 61, 237 (1998).
[9] S. Doniach and S. Engelsberg, Phys. Rev. Lett. **17**, 750 (1966).
[10] N. F. Berk and J. R. Schrieffer, Phys. Rev. Lett. **17**, 433 (1966).
[11] D. J. Scalapino, E. Loh, Jr., and J. E. Hirsch, Phys. Rev. B **34**, 8190 (1986).
[12] K. Miyake,· S. Schmitt-Rink, and C. M. Varma, Phys. Rev. B **34**, 6554 (1986).
[13] N. E. Bickers, D. J. Scalapino and S. R. White, Phys. Rev. Lett. **62**, 961 (1966).
[14] B. Menge and E. Miiller–Hartmann, Z. Phys. B: Cond. Mat. **82**, 237 (1991).
[15] For a review, see, e.g., Y. Yanase, T. Jujo, T. Nomura, H. Ikeda, T. Hotta, K. Yamada, Physics Reports **387**, 1 (2003)

[16] A. I. Lichtenstein, M. I. Katsnelson, Phys. Rev. B **57**, 6884 (1998).
[17] M. Kitatani, N. Tsuji, and H. Aoki, Phys. Rev. B **92**, 085104 (2015).
[18] E. Stenzel and H. Winter, J. Phys. F: Met. Phys. **16**, 1789 (1986).
[19] S. Y. Savrasov, Phys. Rev. Lett. **69**, 2819 (1992).
[20] S. Y. Savrasov, Phys. Rev. Lett. **81**, 2570 (1998).
[21] V. I. Anisimov, J. Zaanen, and O. K. Andersen, Phys. Rev. B **44**, 943 (1991).
[22] V. I. Anisimov, F Aryasetiawan and A. I. Lichtenstein, J. Phys. Condens. Mat. 9, 767 (1997).
[23] J. Gukelberger, L. Huang, and P. Werner, Phys. Rev. B **91**, 235114 (2015).
[24] For a review, see, e..g., E. Gull, A. J. Millis, A. I. Lichtenstein, A. N. Rubtsov, M. Troyer, and P. Werner, Rev. Mod. Phys. *83*, 349 (2011).
[25] A. Ostlin, W. H. Appelt, I. Di Marco, W. Sun, M. Radonjic, M. Sekania, L. Vitos, O. Tjernberg, and L. Chioncel, Phys. Rev. B **93**, 155152 (2016).
[26] In fact, both the LMTO and LAPW methods assume improved projectors that include both the radial wave functions and their energy derivatives in order to better describe orbital partial characters of the one–electron states. See, O. K. Andersen, Phys. Rev. B **12**, 3050 (1975).
[27] K. Haule, Phys. Rev. Lett. **115**, 196403 (2015).
[28] S. Y. Savrasov, Phys. Rev. B **54**, 16470 (1996).
[29] S. H. Vosko, L. Wilk, and M. Nusair, Can. J. Phys. **58**, 1200 (1980).
[30] For a review, see, e.g., F. Yonezawa and K.Morigaki, Prog. Theor. Phys. Supp. **53**, 1 (1973).
[31] G. Resta, S.–T. Pi, X. Wan, S. Y. Savrasov, arXiv:1708.02415.
[32] A. Kutepov, S. Y. Savrasov, and G. Kotliar, Phys. Rev. B **80**, 041103 (2009).
[33] M. van Schilfgaarde, T. Kotani, S. Faleev, Phys. Rev. Lett. **96**, 226402 (2006).
[34] X.Y. Deng, L. Wang, X. Dai, and Z. Fang, Phys. Rev. B **79**, 075114 (2009).
[35] S. Choi, A. Kutepov, K. Haule, M. van Schilfgaarde, G. Kotliar, NPJ Quantum Materials **1**, 16001 (2016).
[36] F. J. Pinski and W. H. Butler, Phys. Rev. B **19**, 6010(1979).
[37] S. Y. Savrasov and D. Y. Savrasov, Phys. Rev. B **54**, 16487 (1996).
[38] K. Haule, C.–H. Yee, and K. Kim, Phys. Rev. B **81**, 195107 (2010).
[39] P. Blaha, K. Schwarz, G. K. H. Madsen, D. Kvasnicka, and J. Luitz, WIEN2K, An Augmented PlaneWave+ Local Orbitals Program for Calculating Crystal Properties (Technische Universitat Wien, Austria, 2001).
[40] K. Haule, Phys. Rev. B **75**, 155113 (2007).
[41] J. F. Janak, Phys. Rev. B **16**, 255 (1977).